1521-0103/12/3421-33–40$25.00
THE JOURNAL OF PHARMACOLOGY AND EXPERIMENTAL THERAPEUTICS Vol. 342, No. 1
Copyright © 2012 by The American Society for Pharmacology and Experimental Therapeutics 192195/3773686
JPET 342:33–40, 2012

Impact of P-Glycoprotein (ABCB1) and Breast Cancer Resistance Protein (ABCG2) on the Brain Distribution of a Novel BRAF Inhibitor: Vemurafenib (PLX4032)

Rajendar K. Mittapalli, Shruthi Vaidhyanathan, Ramola Sane, and William F. Elmquist

Department of Pharmaceutics, Brain Barriers Research Center, University of Minnesota, Minneapolis, Minnesota

Received January 17, 2012; accepted March 26, 2012

ABSTRACT

Vemurafenib [*N*-(3-{[5-(4-chlorophenyl)-1*H*-pyrrolo[2,3-b]pyridin-3-yl]carbonyl}-2,4-difluorophenyl)propane-1-sulfonamide (PLX4032)] is a novel small-molecule BRAF inhibitor, recently approved by the Food and Drug Administration for the treatment of patients with metastatic melanoma with a $BRAF^{V600E}$ mutation. The objective of this study was to investigate the role of P-glycoprotein (P-gp) and breast cancer resistance protein (BCRP) in the distribution of vemurafenib to the central nervous system. In vitro studies conducted in transfected Madin-Darby canine kidney II cells show that the intracellular accumulation of vemurafenib is significantly restricted because of active efflux by P-gp and BCRP. Bidirectional flux studies indicated greater transport in the basolateral-to-apical direction than the apical-to-basolateral direction because of active efflux by P-gp and BCRP. The selective P-gp and BCRP inhibitors zosuquidar and (3*S*,6*S*,12a*S*)-1,2,3,4,6,7,12,12*a*-octahydro-9-methoxy-6-(2-methylpropyl)-1,4-dioxopyrazino(1′,2′:1,6)pyrido(3,4-*b*)indole-3-propanoic acid-1,1-dimethylethyl ester (Ko143) were able to restore the intracellular accumulation and bidirectional net flux of vemurafenib. The in vivo studies revealed that the brain distribution coefficient (area under the concentration time profile of brain/area under the concentration time profile of plasma) of vemurafenib was 0.004 in wild-type mice. The steady-state brain-to-plasma ratio of vemurafenib was 0.035 ± 0.009 in *Mdr1a/b*(−/−) mice, 0.009 ± 0.006 in *Bcrp1*(−/−) mice, and 1.00 ± 0.19 in *Mdr1a/b*(−/−)*Bcrp1*(−/−) mice compared with 0.012 ± 0.004 in wild-type mice. These data indicate that the brain distribution of vemurafenib is severely restricted at the blood-brain barrier because of active efflux by both P-gp and BCRP. This finding has important clinical significance given the ongoing trials examining the efficacy of vemurafenib in brain metastases of melanoma.

Introduction

Melanoma is a neoplasm that originates in the pigment-producing cells of the skin. The incidence of melanoma is escalating. For example, in 2011, approximately 70,000 individuals were expected to be diagnosed with melanoma in the United States, and ~8800 were predicted to die from melanoma (Siegel et al., 2011). After lung and breast cancers, malignant melanoma is the third most common neoplasm that metastasizes to the brain (Johnson and Young, 1996). Approximately 50 to 75% of patients with melanoma are found to have brain metastases at autopsy (Fife et al., 2004). Once the lesions have become established in the central nervous system (CNS) the median survival is less than 6 months (Fife et al., 2004; Raizer et al., 2008).

The current therapeutic options for patients with melanoma include surgery, radiotherapy, chemotherapy, and immunotherapy. The standard therapy using high-dose interleukin-2 and dacarbazine has proven to be unsuccessful in metastatic melanoma, with response rates of only 10 to 20% (Comis, 1976; Atkins et al., 1999; Garbe et al., 2011). The gene encoding the serine-threonine protein kinase BRAF was

This work was supported in part by the National Institutes of Health National Cancer Institute [Grant CA138437]. Financial support for R.S. was provided by the Ronald J. Sawchuk Fellowship in Pharmacokinetics from the Department of Pharmaceutics, University of Minnesota.

R.K.M. and S.V. contributed equally to this work.

Article, publication date, and citation information can be found at http://jpet.aspetjournals.org.
http://dx.doi.org/10.1124/jpet.112.192195.

ABBREVIATIONS: CNS, central nervous system; BBB, blood-brain barrier; P-gp, P-glycoprotein; BCRP, breast cancer resistance protein; ABC, ATP-binding cassette; MDCKII, Madin-Darby canine kidney II; A to B, apical to basolateral; B to A, basolateral to apical; LY335979, (*R*)-4-((1a*R*,6*R*,10b*S*)-1,2-difluoro-1,1a,6,10b-tetrahydrodibenzo-(*a*,*e*)cyclopropa(*c*)cycloheptan-6-yl)-α-((5-quinoloyloxy) methyl)-1-piperazine ethanol, trihydrochloride; PLX4032, *N*-(3-{[5-(4-chlorophenyl)-1*H*-pyrrolo[2,3-b]pyridin-3-yl]carbonyl}-2,4-difluorophenyl)propane-1-sulfonamide; Ko143, (3*S*,6*S*,12a*S*)-1,2,3,4,6,7,12,12*a*-octahydro-9-methoxy-6-(2-methylpropyl)-1,4-dioxopyrazino(1′,2′:1,6)pyrido(3,4-b) indole-3-propanoic acid 1,1-dimethylethyl ester; PLX4720, propane-1-sulfonic acid [3-(5-chloro-1*H*-pyrrolo[2,3-*b*]pyridine-3-carbonyl)-2,4-difluorophenyl]amide; P_{app}, apparent permeability; FVB, Friend leukemia virus strain B; LC-MS/MS, liquid chromatography-tandem mass spectrometry; B/P, brain to plasma; AUC, area under the curve; WT, wild type.

found to be mutated in ~40 to 60% of melanomas (Wan et al., 2004). BRAF is an important component of the RAF/mitogen-activated protein kinase kinase/extracellular signal-regulated kinase signaling pathway, which regulates cell proliferation and growth (McCubrey et al., 2008). The mutated BRAF gene results in signaling pathways that promote tumor cell proliferation, invasion, and resistance. Among the BRAF mutations approximately 80% exhibit a valine-to-glutamic acid substitution (V600E; $BRAF^{V600E}$), resulting in constitutive expression of kinase activity (Davies et al., 2002). A recent study indicated that $BRAF^{V600E}$ is associated with poor patient survival (Long et al., 2011), and further studies show that the incidence of $BRAF^{V600E}$ mutation in brain metastases of melanoma is similar to that found in peripheral sites (Capper et al., 2012). Given the prevalence of $BRAF^{V600E}$ mutations in a large number of melanomas, BRAF has been an attractive treatment target for patients with melanoma who have the V600E mutation, and as such many small-molecule inhibitors of BRAF have been developed.

Vemurafenib (previously known as PLX4032) is a small-molecule $BRAF^{V600E}$ inhibitor that was developed by using a structure-guided drug discovery approach (Tsai et al., 2008). It was approved by the Food and Drug Administration in August 2011 for patients with late-stage melanoma who have the $BRAF^{V600E}$ mutation. Clinical trials with vemurafenib have shown remarkable responses in a high percentage of BRAF mutant melanoma cases (Ribas et al., 2011), with improved overall and progression-free survival (Chapman et al., 2011). A clinical trial evaluating the efficacy of vemurafenib in brain metastases of melanoma is currently recruiting patients (ClinicalTrials.gov identifier NCT01378975). Whether or not vemurafenib will show clinical activity in brain metastases of melanoma is an important question that remains to be answered. In this context, it is crucial to determine the mechanisms influencing the brain distribution of vemurafenib to further support the clinical investigations.

A major factor contributing to the rapid and near 100% mortality in patients with melanoma who have brain metastases has been the presumed limited permeability of chemotherapeutics across the blood-brain barrier (BBB). The BBB is a highly evolved vasculature structure that limits most molecules from distributing into the brain from the blood compartment. Anatomically, the vasculature of the BBB is unique in that it is comprised of endothelial cells that are circumferentially sealed together by tight-junction protein complexes that form the lumen of the vessel. Furthermore, active efflux transporters that are present on the luminal side of capillary endothelium efficiently pump out the drugs from the brain to the blood circulation. ATP-binding cassette (ABC) proteins such as P-glycoprotein (P-gp) and breast cancer resistance protein (BCRP) are major members of the efflux transporters present on the luminal membrane of brain capillary endothelial cells (Schinkel and Jonker, 2003). Studies have shown that many therapeutic agents are substrates of these transporters and, as a result, have very limited brain distribution (Löscher and Potschka, 2005).

Vemurafenib can be considered a "sea change" in the treatment of patients with melanoma. However, important questions still remain regarding resistance and effective delivery to all sites of melanoma metastases, particularly in the brain. In this regard, there is a paucity of data regarding the delivery of antimelanoma agents to brain metastases. Given the remarkable activity of the novel targeted $BRAF^{V600E}$ inhibitors in peripheral disease, it becomes critical to examine the mechanisms that may limit their delivery to brain metastases. Whether vemurafenib can cross the BBB to achieve therapeutic levels in the CNS remains unknown. This has motivated us to examine the interaction of vemurafenib with the two main BBB efflux transporters, P-gp and BCRP. Herein, using in vitro models, we show that vemurafenib is an avid substrate for both P-gp and BCRP. In vivo studies using genetic knockout mice indicate both transporters play a significant role in limiting the CNS distribution of vemurafenib.

Materials and Methods

Chemicals

Vemurafenib (PLX4032) was purchased from Chemietek (Indianapolis, IN). [^{3}H]vinblastine was purchased from Moravek Biochemicals (La Brea, CA). [^{3}H]prazosin was purchased from PerkinElmer Life and Analytical Sciences (Waltham, MA). (3*S*,6*S*,12*aS*)-1,2,3,4,6,7,12,12*a*-octahydro-9-methoxy-6-(2-methylpropyl)-1,4-dioxopyrazino(1′,2′:1,6)pyrido(3,4-*b*)indole-3-propanoic acid-1,1-dimethylethyl ester (Ko143) was a generous gift from Dr. Alfred Schinkel (The Netherlands Cancer Institute, Amsterdam, The Netherlands), and zosuquidar [(*R*)-4-((1*aR*, 6*R*,10*bS*)-1,2-difluoro-1,1*a*,6,10*b*-tetrahydrodibenzo-(*a*,*e*)cyclopropa(*c*)cycloheptan-6-yl)-((5-quinoloyloxy) methyl)-1-piperazine ethanol, trihydrochloride (LY335979)] was kindly provided by Eli Lilly & Co. (Indianapolis, IN). All other chemicals used were of high-performance liquid chromatography or reagent grade and obtained from Sigma-Aldrich (St. Louis, MO).

In Vitro Studies

All in vitro studies were performed by using polarized Madin-Darby canine kidney-II (MDCKII) cells. MDCKII-wild type (WT) and MDR1-transfected (MDCKII-MDR1) cell lines were kindly provided by Dr. Piet Borst (The Netherlands Cancer Institute). MDCKII-WT and Bcrp1-transfected (MDCKII-Bcrp1) cells were a kind gift from Dr. Alfred Schinkel (The Netherlands Cancer Institute). Cells were cultured in Dulbecco's modified Eagle's medium supplemented with 10% (v/v) fetal bovine serum and antibiotics (100 U/ml penicillin, 100 μg/ml streptomycin, and 250 ng/ml amphotericin B). Cells were grown in 25-ml tissue culture-treated flasks before seeding for the experiments and maintained at 37°C in a humidified incubator with 5% CO_2.

In Vitro Accumulation Studies. The intracellular accumulation of vemurafenib was performed in 12-well polystyrene plates (Corning Glassworks, Corning, NY) as described previously (Agarwal et al., 2010, 2011). In brief, cells were seeded at a density of 2×10^5 cells and grown until the cells were ~80% confluent. On the day of experiment the culture media were aspirated, and the cells were washed two times with cell assay buffer (122 mM NaCl, 25 mM $NaHCO_3$, 10 mM glucose, 10 mM HEPES, 3 mM KCl, 2.5 mM $MgSO_4$, 1.8 mM $CaCl_2$, and 0.4 mM K_2HPO_4). Then the cells were preincubated with assay buffer for 30 min, after which the buffer was aspirated and the experiment was initiated by adding 1 ml of vemurafenib (2 μM) to each well with further incubation for 60 min. The assay plates were incubated at 37°C on an orbital shaker (60 rpm) for the entire duration of the experiment. After the incubation period, the drug solution was aspirated, and the cells were washed twice with ice-cold phosphate-buffered saline. Then the cells were lysed by adding 500 μl of 1% Triton X-100 to each well. Four hundred microliters of solubilized cell fraction was sampled from each well, and the concentration of vemurafenib was determined by using liquid chromatography coupled with tandem mass spectrometry (LC-MS/MS) as described below.

Directional Transport across MDKCII Monolayers. The bidirectional flux studies were performed by using six-well Transwell

plates (Corning Life Sciences, Lowell, MA). The cells were seeded at a density of 2×10^5 cells per well, and the media were changed every other day until confluent monolayers were formed. On the day of experiment, the culture medium was aspirated and the cells were washed twice with assay buffer, and after 30-min preincubation, the experiment was initiated by adding the vemurafenib solution (2 μM) in assay buffer to the donor compartment. Samples (200 μl) were collected from the receiver compartment at 0, 30, 60, 90, 120, and 180 min and replaced with drug-free assay buffer. Likewise, at the beginning of the experiment a 200-μl sample was drawn from the donor compartment and replaced with 200 μl of drug solution. The Transwell plates were incubated at 37°C on an orbital shaker for the duration of experiment except for the brief sampling times. When an inhibitor was used, the inhibitor was present in both compartments both before and after the incubation period.

The apparent permeability (P_{app}) for the directional transport was calculated as described previously (Agarwal et al., 2011). The permeabilities were calculated by using the following equation:

$$P_{app} = \frac{dQ}{dt}/(A \times C_0) \quad (1)$$

where dQ/dt is the slope obtained from the initial linear range from the amount transported versus time plot, A is the area of the Transwell membrane, and C_0 is the initial donor concentration. The efflux ratio and corrected efflux ratio were calculated by using eqs. 2 and 3, respectively,

$$\text{Efflux ratio} = \frac{P_{app}(B \rightarrow A)}{P_{app}(A \rightarrow B)} \quad (2)$$

$$\text{Corrected flux ratio} = \frac{\left(\frac{B \rightarrow A}{A \rightarrow B}\right)_{\text{transfected line}}}{\left(\frac{B \rightarrow A}{A \rightarrow B}\right)_{\text{wild-type line}}} \quad (3)$$

where A → B represents permeability in the apical-to-basolateral direction, and B → A represents permeability in the basolateral-to-apical direction.

Competition Assays Using P-gp and Bcrp Probes. Competition assays were performed by using the prototypical probe substrates prazosin for BCRP and vinblastine for P-gp. Intracellular accumulation of these substrates at 60 min was determined in MDCKII-Bcrp1 or MDCKII-MDR1 cells in the presence of different concentrations of vemurafenib ranging from 1 to 25 μM. The increase in probe accumulation relative to control (i.e., no vemurafenib treatment) was reported as a function of vemurafenib concentration.

In Vivo Studies

Animals. All in vivo studies were performed in FVB (wild type), *Mdr1a/b*(−/−) (P-gp knockout), *Bcrp1*(−/−) (BCRP knockout), and *Mdr1a/b*(−/−)*Bcrp1*(−/−) (triple knockout) mice of a FVB genetic background (Taconic Farms, Germantown, NY). All animals were 8 to 10 weeks old at the time of experiment. Animals were maintained in a 12-h light/dark cycle with unlimited access to food and water. The average weight of the mice was ~30 g. All studies were carried out in accordance with the National Institutes of Health's *Guide for the Care and Use of Laboratory Animals* (Institute of Laboratory Animal Resources, 1996) and approved by the Institutional Animal Care and Use Committee of the University of Minnesota.

Brain Distribution of Vemurafenib in FVB Mice. The dosing formulation of vemurafenib was prepared either in a vehicle containing 1% Tween 20 and 1% hydroxyl propyl methyl cellulose (for oral dosing) or a vehicle containing 40% dimethyl sulfoxide, 40% propylene glycol, and 20% saline (for intravenous studies). All vemurafenib formulations were freshly prepared on the day of experiment. In the first study, wild-type, *Mdr1a/b*(−/−), *Bcrp1*(−/−), and *Mdr1a/b*(−/−) *Bcrp1*(−/−) mice received an oral dose of 25 mg/kg, and blood and brain samples were collected 1 and 4 h after dose. At the end of the desired time point, the animals were euthanized by using a CO_2 chamber. Blood was collected via cardiac puncture and collected in heparinized tubes. Plasma was obtained by centrifuging the blood at 7500 rpm for 10 min. Brains were rapidly removed from the skull and rinsed with ice-cold phosphate-buffered saline followed by a flash freeze in liquid nitrogen. Brain and plasma samples were stored at −80°C until further analysis.

In the intravenous dosing study, wild-type and *Mdr1a/b*(−/−) *Bcrp1*(−/−) mice were administered vemurafenib via the tail vein at a dose of 2.5 mg/kg. Blood and brain samples were processed after 5, 30, 90, 180, 300, and 480 min (n = 4 for each time point) as mentioned above.

Steady-State Brain Distribution of Vemurafenib. To determine the steady-state brain and plasma concentrations of vemurafenib, Alzet osmotic minipumps (Durect Corporation, Cupertino, CA) were loaded with vemurafenib (25 mg/ml dissolved in dimethyl sulfoxide) to be released for 48 h at a rate of 1 μl/h. After vemurafenib loading, minipumps were primed overnight in sterile saline at 37°C. Pumps were implanted in the peritoneal cavity of wild-type, *Mdr1a/b*(−/−), *Bcrp1*(−/−), and *Mdr1a/b*(−/−)*Bcrp1*(−/−) mice as described previously (Agarwal et al., 2010, 2011). In brief, mice were anesthetized by using isofluorane, and the abdominal cavity was shaved. A small midline incision was made in the lower abdomen under the rib cage. Then a small incision was made directly in the peritoneal membrane, and the primed pump was inserted in the cavity. The incision was sutured, and the skin was closed by using surgical clips. The animals were allowed to recover on a heating pad and, once recovered, moved to their original cages. The animals were sacrificed 48 h after the implantation of the pumps, and brain and plasma samples were processed as described above.

Analysis of Vemurafenib Using LC-MS/MS. The concentrations of vemurafenib in cell lysates, assay buffer, plasma, and brain homogenate were determined by using a sensitive and specific LC-MS/MS assay. For brains, three volumes of 5% bovine serum albumin was added and homogenized to get a uniform homogenate. For analysis of unknowns, an aliquot of cell lysate, cell assay buffer, brain homogenate, or plasma was spiked with 50 ng of propane-1-sulfonic acid [3-(5-chloro-1*H*-pyrrolo[2,3-*b*]pyridine-3-carbonyl)-2,4-difluorophenyl]amide (PLX4720) as an internal standard and alkalinized by the addition of two volumes of pH 11 buffer (1 mM sodium hydroxide and 0.5 mM sodium bicarbonate). The samples were then extracted by addition of 10 volumes of ethyl acetate followed by vigorous shaking for 5 min and centrifuged at 7500 rpm for 5 min at 4°C to separate the organic layer. The organic layer was transferred to microcentrifuge tubes and dried under nitrogen. Samples were reconstituted in 100 μl of mobile phase and transferred into high-performance liquid chromatography glass vials. Chromatographic analysis was performed by using an AQUITY UPLC system (Waters, Milford, MA). The chromatographic separation was achieved by using an Agilent Technologies (Santa Clara, CA) Eclipse XDB-C18 column (4.6 × 50 mm) with 1.8-μm Zobrax Rx-SIL as the stationary phase. The mobile phase consisted of 20 mM ammonium formate with 0.1% formic acid and acetonitrile (30:70 v/v) and was delivered at a flow rate of 0.25 ml/min.

The column effluent was monitored by using a Waters/Micromass Quattro Ultima mass spectrometer (Waters). The instrument was equipped with an electrospray interface and controlled by the Masslynx (version 4.1) data system (Waters). The samples were analyzed by using an electrospray probe in the negative ionization mode operating at a spray voltage of 2.96 kV for both vemurafenib and PLX4720 (internal standard). Samples were introduced into the interface through a heated nebulized probe where the source and desolvation temperatures were set at 100 and 275°C, respectively. The spectrometer was programmed to allow the [MH]-ion of vemurafenib at m/z 488.23 and that of internal standard at m/z 412.26 to pass through the first quadrupole (Q1) and into the collision cell (Q2). The collision energy was set at 27 V for vemurafenib and 25 V for PLX4720. The product ions for vemurafenib (m/z 380.89) and the

internal standard PLX4720 (m/z 304.82) were monitored through the third quadrupole (Q3). The retention times for vemurafenib and the internal standard PLX4720 were 4.2 and 2.9 min, respectively. The assay was sensitive and linear over a range of 1.2 ng/ml to 1.2 μg/ml, with the coefficient of variation being less than 15% over the entire range.

Pharmacokinetic Calculations

Pharmacokinetic parameters and metrics were calculated by noncompartmental methods using Phoenix WinNonlin (version 6.1) (Pharsight, Mountain View, CA). The area under the concentration time curve in both plasma and brain was calculated by using the trapezoidal rule, and the area under the curve was determined up to the last measured time point ($AUC_{0\text{-tlast}}$). $AUC_{0\text{-tlast}}$ was used in determining brain-to-plasma (B/P) distribution ratio. The area under the curve from time 0 to infinity was also determined, and the area extrapolated was less than 20% of the total area under the concentration curve. The terminal rate constants were determined by using all of the data points in the brain and the last three data points in the plasma. In plasma, the concentration at zero time was extrapolated by using the terminal rate constant to measure the area under the curve at time 0 to the first measured time point.

Statistical Analysis

Data in all experiments represent mean ± S.D. unless otherwise indicated. Comparisons between two groups were made by using an unpaired t test. One-way analysis of variance, followed by Bonferonni's multiple comparisons test, was used to compare multiple groups. A significance level of $p < 0.05$ was used for all experiments (Prism 5.01; GraphPad Software Inc., San Diego, CA).

Results

Intracellular Accumulation of Vemurafenib. The intracellular accumulation of vemurafenib was studied in MDCKII WT and P-gp- or Bcrp-overexpressing cell lines. [^{3}H]prazosin and [^{3}H]vinblastine were used as positive controls for Bcrp and P-gp, respectively. As expected, the accumulation of [^{3}H]prazosin (Fig. 1A) was significantly lower in the Bcrp-overexpressing cell lines (WT, 100.0 ± 19.5; Bcrp, 14.0 ± 5.0, $p < 0.0001$). Likewise, the accumulation of [^{3}H]vinblastine (Fig. 1B) in P-gp-overexpressing cells was ~80% lower compared with its WT line (WT, 100.0 ± 24.0; MDR1, 13.8 ± 4.1, $p = 0.0004$). Vemurafenib accumulation was ~ 77% lower in the Bcrp-overexpressing cell line compared with its WT line (WT, 100.0 ± 5.0; Bcrp, 12.9 ± 0.3; $P < 0.0001$). The difference in accumulation was abolished when a specific Bcrp inhibitor, Ko143, was added (Bcrp, 12.9 ± 0.3; Bcrp with Ko143, 69.8 ± 3.0; $p < 0.05$). Likewise, the accumulation of vemurafenib was ~20% lower in the P-gp-overexpressing line compared with its WT control (WT, 100.0 ± 2.6; MDR1, 73.6 ± 5.5; $p < 0.05$), and the difference in accumulation was abolished (Fig. 1B) when a specific P-gp inhibitor, LY335979, was added (MDR1, 73.6 ± 5.5; MDR1 with LY335979, 110.8 ± 2.9). The aggregate of these data indicates that vemurafenib is a substrate for both P-gp and Bcrp in vitro.

Competition Assays. The in vitro competition assays for vemurafenib were performed in MDCKII cells by using vinblastine and prazosin as P-gp and Bcrp prototype probe substrates, respectively. The addition of increasing concentrations of vemurafenib resulted in a gradual increase in the accumulation of prazosin and vinblastine in MDCKII-Bcrp1 cells and MDCKII-MDR1 cells, respectively. The fold increase in prazosin accumulation in MDCKII-Bcrp1 cells at 10 μM vemurafenib was no different from the effect seen with 0.2 μM Ko143, a potent Bcrp inhibitor (Fig. 2A). Likewise, at 25 μM vemurafenib, the fold increase in vinblastine accumulation was no different from the effect seen with the potent P-gp inhibitor LY335959 (Fig. 2B) in MDCKII-MDR1 cells. These data suggest that vemurafenib may share the same binding sites on the transporter proteins as these prototypical probe substrates.

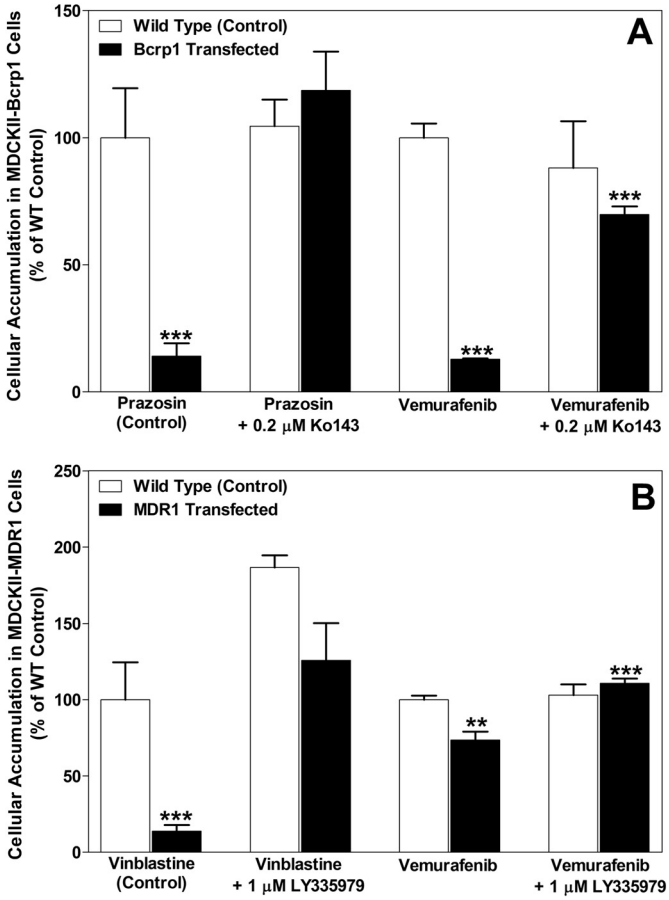

Fig. 1. Intracellular accumulation of vemurafenib in MDCKII cells. A, accumulation of vemurafenib is significantly lower in Bcrp-transfected lines compared with its WT control. The difference in accumulation was abolished when a specific Bcrp inhibitor, Ko143, was used. B, the accumulation of vemurafenib is ~20% less in MDR1-transfected cells than the WT controls, and the difference was abolished when the MDR1-specific inhibitor LY335979 was used. Data represent mean ± S.D. (n = 3–6 for all data sets). **, $p < 0.01$; ***, $p < 0.0001$.

Bidirectional Flux across MDCKII Monolayers. The in vitro transport (A to B and B to A) of vemurafenib was studied in MDCKII wild-type and P-gp- or Bcrp-overexpressing cell lines. Figure 3, A and B demonstrates the transport of vemurafenib in the A-to-B and B-to-A direction in Bcrp1 and corresponding wild-type cell monolayers. In the wild-type cells, there was minimal transport (less than 2.3% in 1.5 h) of vemurafenib in either direction (Fig. 3A). In the case of the MDCKII-Bcrp1 cells, the permeability of vemurafenib in the B-to-A direction was significantly higher than the permeability in the A-to-B direction (A to B, $0.02 \pm 0.003 \times 10^{-6}$ cm/s; B to A, $9.9 \pm 6.8 \times 10^{-6}$ cm/s; $p < 0.05$; Fig. 3C). The addition of 0.2 μM Ko143, a specific Bcrp inhibitor, resulted in partial inhibition of Bcrp-mediated vemurafenib transport in these cells (Fig. 3C).

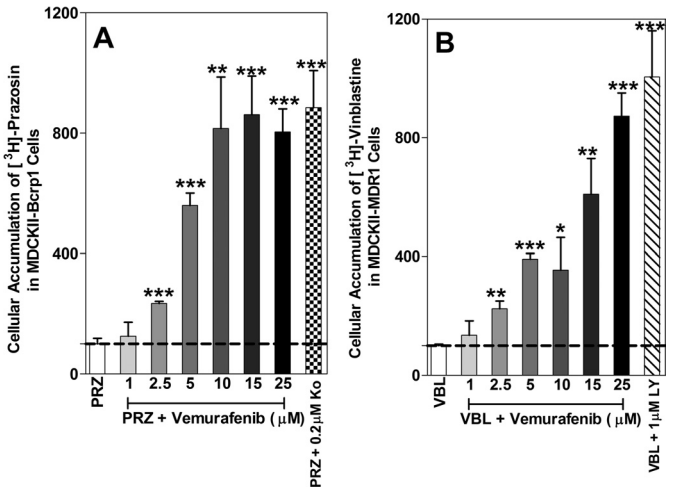

Fig. 2. Competition assays for vemurafenib in MDCKII-MDR1 and MDCKII-Bcrp1 cells by using [^{3}H]vinblastine (VBL) and [^{3}H]prazosin (PRZ) as P-gp and Bcrp prototypical probe substrates, respectively. The addition of increasing concentrations of vemurafenib resulted in an increased accumulation of [^{3}H]prazosin and [^{3}H]vinblastine in Bcrp1 (A) and MDR1 (B) cells, respectively. The data represent mean ± S.D. (n = 3 for all data sets). *, $p < 0.05$; **, $p < 0.01$; ***, $p < 0.0001$.

The transport of vemurafenib in the A-to-B and B-to-A directions in MDR1 and corresponding wild-type cell monolayers is depicted in Fig. 3, D and E. In the case of the MDCKII-MDR1-transfected line, the permeability of vemurafenib in the B-to-A direction was significantly greater compared with permeability in the A-to-B direction (A to B, $0.21 \pm 0.16 \times 10^{-6}$ cm/s; B to A, $16.7 \pm 2.1 \times 10^{-6}$ cm/s; $p < 0.05$; Fig. 3F), resulting in an efflux ratio of ~80. The addition of 1 μM LY335979, a potent inhibitor of P-gp, resulted in partial inhibition of P-gp-mediated vemurafenib transport in these cell lines (Fig. 3F). The B-to-A permeability of vemurafenib was not significantly different from the A-to-B permeability in the corresponding wild-type cells. The corrected flux ratio was found to be approximately 34 in control and 2 in cells treated with the P-gp inhibitor LY335979.

Brain Distribution of Vemurafenib in FVB Wild-Type and *Mdr1a/b*(−/−)*Bcrp1*(−/−) Mice after Intravenous Administration. The brain distribution of vemurafenib was studied in FVB wild-type mice after an intravenous dose of 2.5 mg/kg via the tail vein. Figure 4 shows the concentration time profile of vemurafenib in both plasma and brain at 5, 30, 90, 180, 300, and 480 min after intravenous dose. The plasma concentrations of vemurafenib

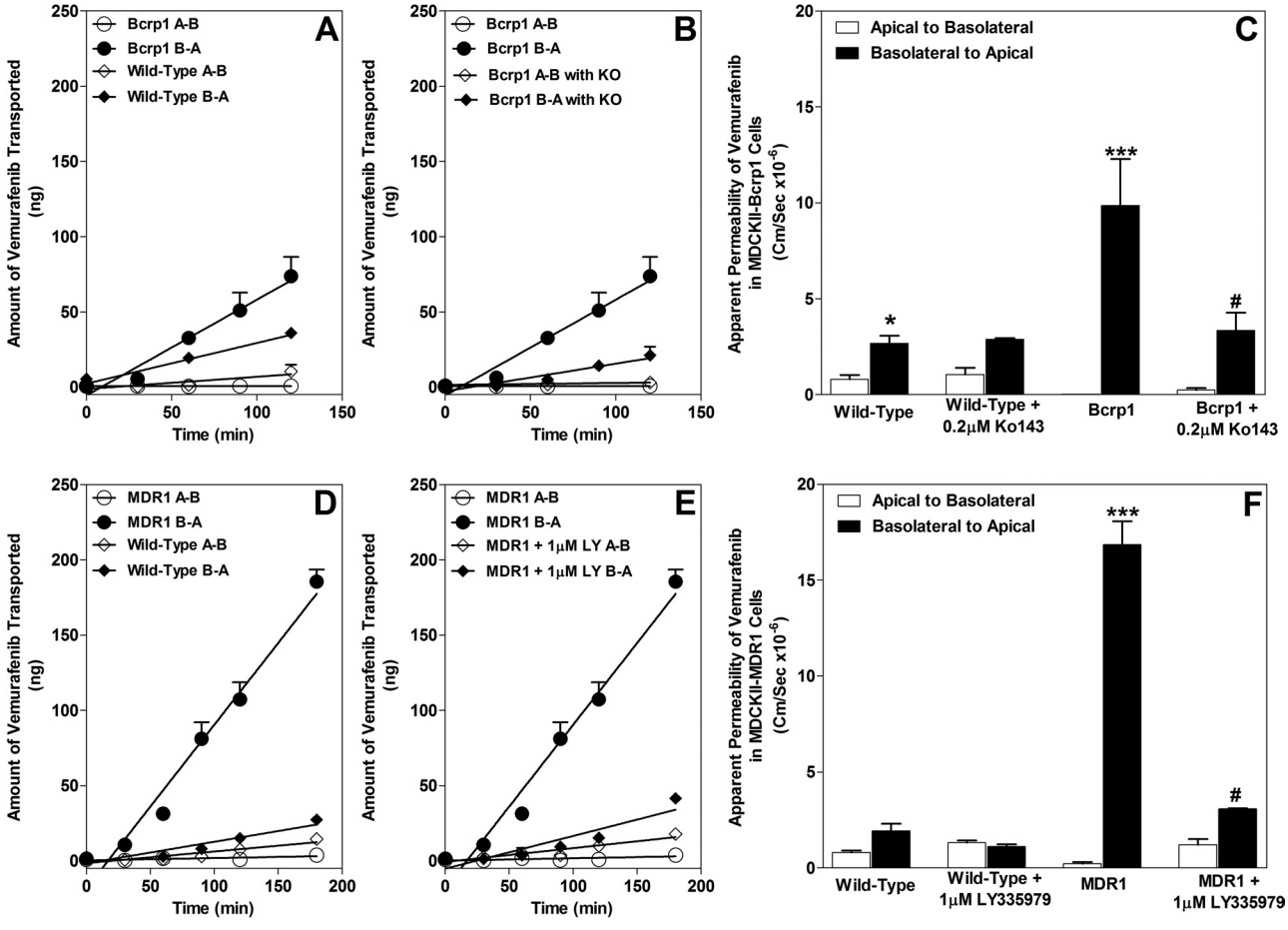

Fig. 3. Directional flux of vemurafenib in MDCKII cell monolayers. A and B, the transport of vemurafenib in wild-type (A) and Bcrp1-transfected (B) cells. KO, Ko143. C, the apparent permeability of vemurafenib in wild-type and Bcrp1 cells in both the A-to-B and B-to-A directions. In the Bcrp1-transfected cells, the B-to-A permeability of vemurafenib was significantly greater than the A-to-B permeability (***, $p < 0.05$). The addition of 0.2 μM Ko143, a potent Bcrp inhibitor, decreased this directionality in flux caused by Bcrp (#, $p < 0.05$). D and E, the transport of vemurafenib in wild-type (D) and MDR1-transfected (E) cells. LY, LY335979. F, the apparent permeability of vemurafenib in wild-type and MDR1 cells in both the A-to-B and B-to-A directions. In the MDR1-transfected cells, the B-to-A permeability of vemurafenib was significantly greater than the A-to-B permeability (***, $p < 0.05$). The addition of 1 μM LY335979, a potent P-gp inhibitor, abolished this directionality in flux caused by P-gp (#, $p < 0.05$), such that there was no significant difference in the permeability of vemurafenib in both directions. Data represent mean ± S.E. (n = 3–9 for all data sets).

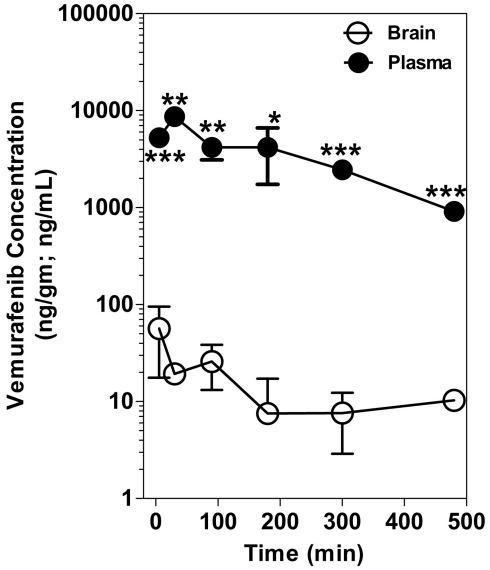

Fig. 4. Brain and plasma concentrations of vemurafenib after an intravenous dose of 2.5 mg/kg in FVB wild-type mice. Whole brain and plasma were collected at 5, 30, 90, 180, 300, and 480 min after dose and were analyzed by LC-MS/MS. The brain concentrations of vemurafenib were significantly lower than the plasma concentrations at all time points. *, $p < 0.05$; **, $p < 0.01$; ***, $p < 0.0001$. Data are mean ± S.D. (n = 3–4 for all data points).

TABLE 1

Vemurafenib pharmacokinetic parameters after an intravenous dose of 2.5 mg/kg in FVB wild-type mice

Plasma and brain pharmacokinetic parameters were analyzed by using noncompartmental analysis after an intravenous dose of 2.5 mg/kg in FVB wild-type mice. The AUC_{brain} to AUC_{plasma} ratio of 0.004 indicates the severely restricted brain distribution of vemurafenib.

	Plasma	Brain
Terminal rate constant, min^{-1}	0.0051	0.0047
Half-life, min	136	148
Clearance, ml/min	0.04	
Volume of distribution, ml	7.9	
$AUC_{0\rightarrow tlast}$, min · μg/ml	1663 ± 140*	6.5 ± 0.9*
AUC_{Brain}/AUC_{Plasma}	0.004	

* Mean ± S.E. (standard error of the estimate).

were significantly higher (~3 log units) at all time points compared with its brain concentrations, indicating the severely restricted brain distribution of vemurafenib. The brain-to-plasma partitioning (AUC_{brain}/AUC_{plasma}) was found to be ~0.004 in FVB wild-type mice. The pharmacokinetic parameters are depicted in Table 1.

In a separate study, the brain distribution of vemurafenib in *Mdr1a/b*(−/−)*Bcrp1*(−/−) mice was examined after an intravenous dose of 2.5 mg/kg. As shown in Fig. 5B, the brain concentrations of vemurafenib in *Mdr1a/b*(−/−)*Bcrp1*(−/−) mice were significantly higher than in wild-type mice. The plasma concentrations were not different between the two types of mice (Fig. 5A). The B/P ratio of vemurafenib in wild-type mice was ~0.4%, significantly lower than the B/P ratio in *Mdr1a/b*(−/−)*Bcrp1*(−/−) mice (Fig. 5C).

Brain Distribution of Vemurafenib after Oral Administration. The brain distribution of vemurafenib was examined 1 and 4 h after oral doses (25 mg/kg) of vemurafenib in FVB wild-type, *Mdr1a/b*(−/−), *Bcrp1*(−/−), and *Mdr1a/b*(−/−)*Bcrp1*(−/−) mice. As shown in Fig. 6A, the brain concentrations of vemurafenib were significantly lower than plasma 1 h after dose in wild-type, *Mdr1a/b*(−/−), and *Bcrp1*(−/−) mice with a B/P ratio of <0.02. It should be noted that the brain concentrations were not corrected for the vascular content because the total brain distribution of vemurafenib was approximately equal to the vascular volume, indicating the very limited brain distribution of vemurafenib. However, the B/P ratio of vemurafenib was significantly ($p < 0.0001$) higher in *Mdr1a/b*(−/−)*Bcrp1*(−/−) mice (Fig. 6; B/P ratio at 1 h, 0.090 ± 0.036; at 4 h, 0.36 ± 0.07) than the wild-type and single knockout mice at both 1 and 4 h after dose. It is noteworthy that the B/P ratio of *Mdr1a/b*(−/−)*Bcrp1*(−/−) mice was 8-fold higher than wild type at 1 h and 30-fold higher than wild type at 4 h. These data show the important roles of both P-gp and Bcrp in restricting the delivery of vemurafenib across the BBB.

Steady-State Brain Distribution of Vemurafenib. The steady-state brain distribution of vemurafenib was studied after a constant intraperitoneal infusion by using the Alzet osmotic pumps for 48 h. As shown in Fig. 7A, the steady-state brain concentrations of vemurafenib were significantly lower in wild-type, *Mdr1a/b*(−/−), and *Bcrp1*(−/−) mice compared with their respective steady-state plasma concentrations. The steady-state B/P plasma ratio of vemurafenib in *Mdr1a/b*(−/−) *Bcrp1*(−/−) mice equaled approximately 1 (Fig. 7B), which is 80-fold ($p < 0.0001$) greater than the wild-type and single knockout mice [wild type, 0.012 ± 0.004; *Mdr1a/b*(−/−), 0.035 ± 0.009; *Bcrp1*(−/−), 0.009 ± 0.006; *Mdr1a/b*(−/−)*Bcrp1*(−/−), 1.00 ± 0.19].

Discussion

The development of vemurafenib, a potent $BRAF^{V600E}$ inhibitor, yields new hope for the patients with melanoma who harbor this mutational status. However, the durable efficacy of vemurafenib depends on overcoming resistance (Wagle et al., 2011) and ensuring adequate delivery to all sites of metastases in patients with melanoma, particularly the brain. Given the remarkable success in the early clinical trials (Chapman et al., 2011; Ribas et al., 2011), it is of particular interest to examine mechanisms that may limit the CNS distribution of vemurafenib to support further clinical trials. In the current study, we have evaluated how BBB efflux transporters influence the CNS distribution of vemurafenib by using both in vitro cell culture models and in vivo models with genetic knockout mice. We demonstrate that vemurafenib is a substrate for the ABC transporters P-gp and BCRP, and active efflux by these two transporters at the BBB severely restricts the CNS distribution of vemurafenib.

Studies performed in vitro with MDCKII cells that overexpress human P-gp or murine BCRP revealed that vemurafenib is an avid substrate for the two efflux transporters. Using prototypical probe substrates (prazosin for BCRP and vinblastine for P-gp), we have seen a concentration-dependent increase in cellular accumulation of the probe substrate with increasing concentrations of vemurafenib. We have examined the vectorial transport of vemurafenib across monolayers formed from MDCKII wild-type, MDCKII-MDR1-transfected, and MDCKII-Bcrp1-transfected cells. The corrected flux ratio for vemurafenib in the MDR1-transfected line was ~34, and the ratio in the BCRP-transfected line was 150, indicating that vemurafenib is subject to significant efflux by each transporter across the monolayers. The selective P-gp and BCRP inhibitors zosuquidar and Ko143 were able to restore the

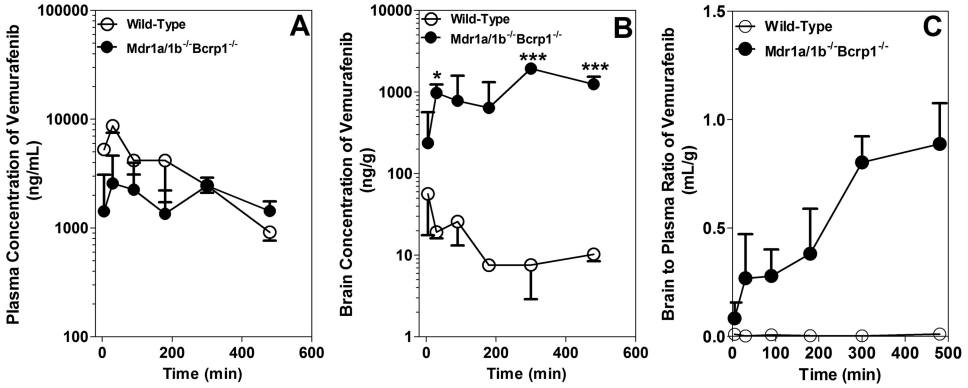

Fig. 5. Comparison of vemurafenib brain distribution in wild-type and *Mdr1a/b*(−/−) *Bcrp1*(−/−) mice. Vemurafenib was given intravenously at 2.5 mg/kg, and the concentrations in brain and plasma were determined by LC-MS/MS. A and B, the plasma (A) and brain (B) concentrations of vemurafenib in wild-type and *Mdr1a/b*(−/−)*Bcrp1*(−/−) mice. C, the B/P ratio for vemurafenib in wild-type and *Mdr1a/b*(−/−)*Bcrp1*(−/−) mice. Data represent mean ± S.D. (n = 3–4 for all data points).

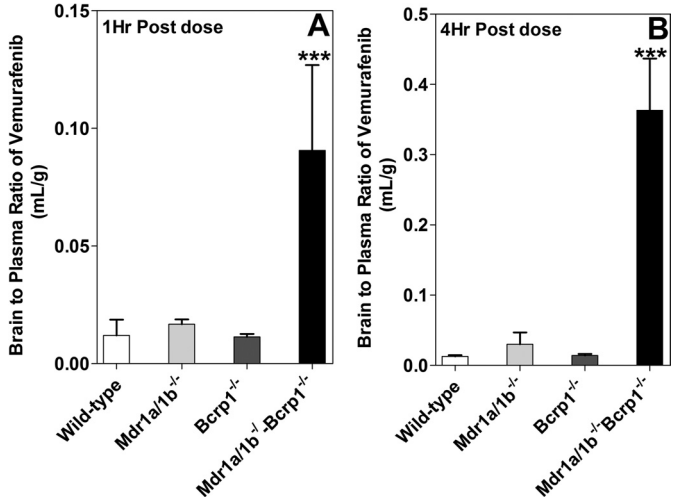

Fig. 6. Brain-to-plasma ratios of vemurafenib after an oral dose of 25 mg/kg in FVB wild-type, *Mdr1a/b*(−/−), *Bcrp1*(−/−), and *Mdr1a/b*(−/−) *Bcrp1*(−/−) mice. The mice were sacrificed after 1 h (A) and 4 h (B) postdose of vemurafenib, and whole brain and plasma were analyzed by LC-MS/MS. The B/P ratios were significantly higher in *Mdr1a/b*(−/−)*Bcrp1*(−/−) mice than the wild-type mice at both 1 and 4 h postdose. ***, $p < 0.0001$. Data are mean ± S.D. (n = 3–4 for all data points).

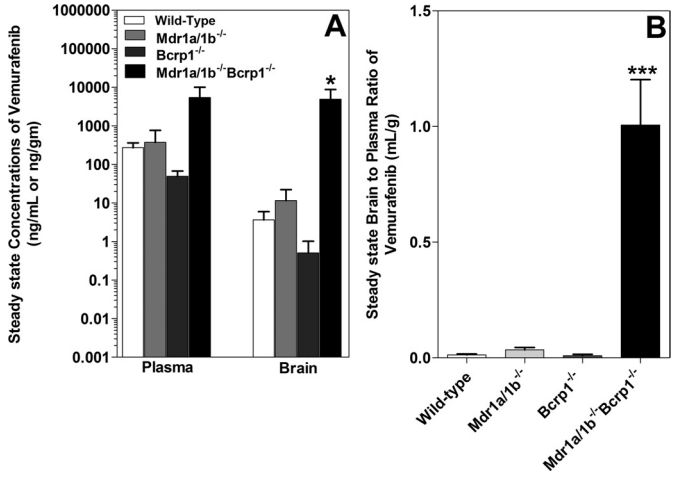

Fig. 7. Steady-state brain distribution of vemurafenib in FVB wild-type, *Mdr1a/b*(−/−) (P-gp knockout), *Bcrp1*(−/−) (BCRP knockout), and *Mdr1a/b*(−/−)*Bcrp1*(−/−) (triple knockout) mice. Vemurafenib was delivered at a constant infusion for 48 h at a rate of 25 μg/h, and the brain and plasma concentrations were determined thereafter. A, the steady-state brain and plasma concentrations of vemurafenib. B, the B/P ratio in all four types of mice. The B/P ratios were not significantly different in single knockout mice compared with wild-type mice. However, the B/P ratio in triple knockout mice was significantly higher than the wild-type mice, indicating the cooperative role of P-gp and Bcrp at the blood-brain barrier. *, $p < 0.05$; ***, $p < 0.0001$. Data are mean ± S.D. (n = 3–4 for all data points).

intracellular accumulation and bidirectional net flux of vemurafenib. These in vitro results conclusively show that vemurafenib is a substrate for these two efflux transporters.

In vivo studies using FVB wild-type mice demonstrated that the CNS distribution of vemurafenib is significantly restricted across the blood-brain barrier. The brain concentrations of vemurafenib in FVB wild-type mice were significantly (~3 log units; Fig. 4) lower than the plasma concentrations. However, the brain concentrations were approximately ~8- to 30-fold higher in *Mdr1a/b*$^{(-/-)}$ *Bcrp1*(−/−) mice than in the wild-type mice (Fig. 6). Steady-state brain-to-plasma ratios increased from approximately 0.01 in the wild-type mice to approximately 1 in the triple knockout mice. This remarkable 80-fold increase in the targeted brain distribution of vemurafenib in *Mdr1a/b*(−/−)*Bcrp1*(−/−) mice indicates the significant impact of P-gp and BCRP on CNS penetration of vemurafenib. It should be noted that the brain distribution of vemurafenib did not increase in *Bcrp1*(−/−) mice; it is increased by ~3-fold in *Mdr1a/b*(−/−) mice, indicating the "cooperative" role of these transporters at BBB. This type of "synergistic" effect of P-gp and BCRP was seen with other drugs; such as topotecan (de Vries et al., 2007), lapatinib (Polli et al., 2009), dasatinib (Chen et al., 2009), gefitinib (Agarwal et al., 2010), and sorafenib (Agarwal et al., 2011). There are a number of underlying assumptions for this disproportional increase in brain distribution of compounds in triple knockout mice. The first assumption is that there is no change in the expression of other transporters at the BBB in these mice. Compensatory up- or down-regulation of active efflux and influx transporters in single knockout mice (mice lacking either P-gp or BCRP) could explain some of the findings in the P-gp/BCRP knockout mice. However, in our previous study, using a quantitative proteomics approach, we have shown no compensatory changes in the BBB expression of relevant transporters in the single and combined knockout mice (Agarwal et al., 2012). The exact functional compensation between P-gp and BCRP at the BBB needs further investigation.

Although vemurafenib shows high initial response rates in patients with melanoma who have the BRAF^{V600E} mutation and has been shown to yield a durable response in a melanoma brain metastasis in one recent case study (Rochet, 2011), the development of resistance can occur quickly (Wagle et al., 2011). At the present time, several resistance mechanisms against BRAF inhibitors have been documented, some of which include the up-regulation of neuroblastoma RAS, platelet-derived growth factor receptor, and insulin-like growth factor receptor 1/phosphatidylinositol

3-kinase signaling (Johannessen et al., 2010; Nazarian et al., 2010; Villanueva et al., 2010). Therefore, the development of more effective combination therapies has been suggested (Vultur et al., 2011; Ji et al., 2012). In this context, the interaction of drugs such as vemurafenib with ABC transporters could be of great relevance for the rational design of therapeutic strategies in the clinical setting. In the current study, we have shown that the brain distribution of vemurafenib is severely restricted at the blood-brain barrier because of active efflux by both P-gp and BCRP. This finding is clinically significant considering the ongoing trials on the efficacy of vemurafenib in brain metastases of melanoma.

Given the remarkable success thus far with vemurafenib, it will be crucial to find both the drug resistance and drug delivery liabilities to further improve progression-free survival rates through rational drug development and design. In this particular case, the lack of treatment options and the aggressive course of this malignancy suggest that adjuvant treatment to improve delivery to the CNS through efflux inhibition may be a viable option for improving survival.

Acknowledgments

We thank Jim Fisher (Clinical Pharmacology Analytical Services Laboratory, University of Minnesota, Minneapolis, Minnesota) for help and support in the development of the vemurafenib LC-MS/MS assay.

Authorship Contributions

Participated in research design: Mittapalli, Vaidhyanathan, Sane, and Elmquist.

Conducted experiments: Mittapalli, Vaidhyanathan, and Sane.

Performed data analysis: Mittapalli and Elmquist.

Wrote or contributed to the writing of the manuscript: Mittapalli, Vaidhyanathan, and Elmquist.

References

Agarwal S, Sane R, Gallardo JL, Ohlfest JR, and Elmquist WF (2010) Distribution of gefitinib to the brain is limited by P-glycoprotein (ABCB1) and breast cancer resistance protein (ABCG2)-mediated active efflux. *J Pharmacol Exp Ther* **334:** 147–155.

Agarwal S, Sane R, Ohlfest JR, and Elmquist WF (2011) The role of the breast cancer resistance protein (ABCG2) in the distribution of sorafenib to the brain. *J Pharmacol Exp Ther* **336:**223–233.

Agarwal S, Uchida Y, Mittapalli RK, Sane R, Terasaki T, and Elmquist WF (2012) Quantitative proteomics of transporter expression in brain capillary endothelial cells isolated from P-gp, BCRP, and P-gp/BCRP knockout mice. *Drug Metab Dispos* http://dx.doi.org/10.1124/dmd.112.044719.

Atkins MB, Lotze MT, Dutcher JP, Fisher RI, Weiss G, Margolin K, Abrams J, Sznol M, Parkinson D, Hawkins M, et al. (1999) High-dose recombinant interleukin 2 therapy for patients with metastatic melanoma: analysis of 270 patients treated between 1985 and 1993. *J Clin Oncol* **17:**2105–2116.

Capper D, Berghoff AS, Magerle M, Ilhan A, Wöhrer A, Hackl M, Pichler J, Pusch S, Meyer J, Habel A, et al. (2012) Immunohistochemical testing of BRAF V600E status in 1,120 tumor tissue samples of patients with brain metastases. *Acta Neuropathol* **123:**223–233.

Chapman PB, Hauschild A, Robert C, Haanen JB, Ascierto P, Larkin J, Dummer R, Garbe C, Testori A, Maio M, et al. (2011) Improved survival with vemurafenib in melanoma with BRAF V600E mutation. *N Engl J Med* **364:**2507–2516.

Chen Y, Agarwal S, Shaik NM, Chen C, Yang Z, and Elmquist WF (2009) P-glycoprotein and breast cancer resistance protein influence brain distribution of dasatinib. *J Pharmacol Exp Ther* **330:**956–963.

Comis RL (1976) DTIC (NSC-45388) in malignant melanoma: a perspective. *Cancer Treat Rep* **60:**165–176.

Davies H, Bignell GR, Cox C, Stephens P, Edkins S, Clegg S, Teague J, Woffendin H, Garnett MJ, Bottomley W, et al. (2002) Mutations of the BRAF gene in human cancer. *Nature* **417:**949–954.

de Vries NA, Zhao J, Kroon E, Buckle T, Beijnen JH, and van Tellingen O (2007) P-glycoprotein and breast cancer resistance protein: two dominant transporters working together in limiting the brain penetration of topotecan. *Clin Cancer Res* **13:**6440–6449.

Fife KM, Colman MH, Stevens GN, Firth IC, Moon D, Shannon KF, Harman R, Petersen-Schaefer K, Zacest AC, Besser M, et al. (2004) Determinants of outcome in melanoma patients with cerebral metastases. *J Clin Oncol* **22:**1293–1300.

Garbe C, Eigentler TK, Keilholz U, Hauschild A, and Kirkwood JM (2011) Systematic review of medical treatment in melanoma: current status and future prospects. *Oncologist* **16:**5–24.

Institute of Laboratory Animal Resources (1996) *Guide for the Care and Use of Laboratory Animals* 7th ed. Institute of Laboratory Animal Resources, Commission on Life Sciences, National Research Council, Washington, DC.

Ji Z, Flaherty KT, and Tsao H (2012) Targeting the RAS pathway in melanoma. *Trends Mol Med* **18:**27–35.

Johannessen CM, Boehm JS, Kim SY, Thomas SR, Wardwell L, Johnson LA, Emery CM, Stransky N, Cogdill AP, Barretina J, et al. (2010) COT drives resistance to RAF inhibition through MAP kinase pathway reactivation. *Nature* **468:**968–972.

Johnson JD and Young B (1996) Demographics of brain metastasis. *Neurosurg Clin N Am* **7:**337–344.

Long GV, Menzies AM, Nagrial AM, Haydu LE, Hamilton AL, Mann GJ, Hughes TM, Thompson JF, Scolyer RA, and Kefford RF (2011) Prognostic and clinicopathologic associations of oncogenic BRAF in metastatic melanoma. *J Clin Oncol* **29:**1239–1246.

Löscher W and Potschka H (2005) Blood-brain barrier active efflux transporters: ATP-binding cassette gene family. *NeuroRx* **2:**86–98.

McCubrey JA, Milella M, Tafuri A, Martelli AM, Lunghi P, Bonati A, Cervello M, Lee JT, and Steelman LS (2008) Targeting the Raf/MEK/ERK pathway with small-molecule inhibitors. *Curr Opin Investig Drugs* **9:**614–630.

Nazarian R, Shi H, Wang Q, Kong X, Koya RC, Lee H, Chen Z, Lee MK, Attar N, Sazegar H, et al. (2010) Melanomas acquire resistance to B-RAF(V600E) inhibition by RTK or N-RAS upregulation. *Nature* **468:**973–977.

Polli JW, Olson KL, Chism JP, John-Williams LS, Yeager RL, Woodard SM, Otto V, Castellino S, and Demby VE (2009) An unexpected synergist role of P-glycoprotein and breast cancer resistance protein on the central nervous system penetration of the tyrosine kinase inhibitor lapatinib (*N*-{3-chloro-4-[(3-fluorobenzyl)oxy]phenyl}-6-[5-({[2-(methylsulfonyl)ethyl]amino}methyl)-2-furyl]-4-quinazolinamine; GW572016). *Drug Metab Dispos* **37:**439–442.

Raizer JJ, Hwu WJ, Panageas KS, Wilton A, Baldwin DE, Bailey E, von Althann C, Lamb LA, Alvarado G, Bilsky MH, et al. (2008) Brain and leptomeningeal metastases from cutaneous melanoma: survival outcomes based on clinical features. *Neuro Oncol* **10:**199–207.

Ribas A, Kim K, Schuchter L, Gonzalez R, Pavlick AC, Weber JS, McArthur GA, Hutson TE, Flaherty KT, Moschos SJ, et al. (2011) BRIM-2: An open-label, multicenter phase II study of vemurafenib in previously treated patients with BRAF V600E mutation-positive metastatic melanoma. *J Clin Oncol* **29 (Suppl):**8509.

Rochet NM, Kottschade LA, and Markovic SN (2011) Vemurafenib for Melanoma Metastases to the Brain. *N Engl J Med* **365:**2439–2441.

Schinkel AH and Jonker JW (2003) Mammalian drug efflux transporters of the ATP binding cassette (ABC) family: an overview. *Adv Drug Deliv Rev* **55:**3–29.

Siegel R, Ward E, Brawley O, and Jemal A (2011) Cancer statistics, 2011: the impact of eliminating socioeconomic and racial disparities on premature cancer deaths. *CA Cancer J Clin* **61:**212–236.

Tsai J, Lee JT, Wang W, Zhang J, Cho H, Mamo S, Bremer R, Gillette S, Kong J, Haass NK, et al. (2008) Discovery of a selective inhibitor of oncogenic B-Raf kinase with potent antimelanoma activity. *Proc Natl Acad Sci U S A* **105:**3041–3046.

Villanueva J, Vultur A, Lee JT, Somasundaram R, Fukunaga-Kalabis M, Cipolla AK, Wubbenhorst B, Xu X, Gimotty PA, Kee D, et al. (2010) Acquired resistance to BRAF inhibitors mediated by a RAF kinase switch in melanoma can be overcome by cotargeting MEK and IGF-1R/PI3K. *Cancer Cell* **18:**683–695.

Vultur A, Villanueva J, and Herlyn M (2011) Targeting BRAF in advanced melanoma: a first step toward manageable disease. *Clin Cancer Res* **17:**1658–1663.

Wagle N, Emery C, Berger MF, Davis MJ, Sawyer A, Pochanard P, Kehoe SM, Johannessen CM, Macconaill LE, Hahn WC, et al. (2011) Dissecting therapeutic resistance to RAF inhibition in melanoma by tumor genomic profiling. *J Clin Oncol* **29:**3085–3096.

Wan PT, Garnett MJ, Roe SM, Lee S, Niculescu-Duvaz D, Good VM, Jones CM, Marshall CJ, Springer CJ, Barford D, et al. (2004) Mechanism of activation of the RAF-ERK signaling pathway by oncogenic mutations of B-RAF. *Cell* **116:**855–867.

Address correspondence to: William F. Elmquist, Department of Pharmaceutics, University of Minnesota, 9-177 Weaver Densford Hall, 308 Harvard Street SE, Minneapolis, MN 55455. E-mail: elmqu011@umn.edu